Earth and Space Science

RESEARCH ARTICLE
10.1029/2020EA001474

Special Section:
Forecast model fidelity for extreme weather

Performance of RegCM4 for Dynamically Downscaling of El Nino/La Nina Events During Southwest Monsoon Over India and Its Regions

Shruti Verma[1] and **R. Bhatla**[1,2]

[1]Department of Geophysics, Institute of Science, Banaras Hindu University, Varanasi, India, [2]DST-Mahamana Centre of Excellence in Climate Change Research, Institute of Environment and Sustainable Development, Banaras Hindu University, Varanasi, India

Key Points:

- The modulation of spatial and temporal south west monsoon rainfall during ENSO phases are prominent
- El Nino and La Nina episodes control the probability of occurrences and length of wet spell and dry spell during monsoon
- The skill of RegCM4 in simulating ISMR during the extreme ENSO phases are better in "dry" conditions rather below average for the accurate simulation of "wet" conditions

Correspondence to:
S. Verma,
shrutiverma072@gmail.com;
shruti.verma@bhu.ac.in

Citation:
Verma, S., & Bhatla, R. (2021). Performance of RegCM4 for dynamically downscaling of El Nino/La Nina events during southwest monsoon over India and its regions. *Earth and Space Science*, *8*, e2020EA001474. https://doi.org/10.1029/2020EA001474

Received 24 SEP 2020
Accepted 16 JAN 2021

Abstract This study presents the interannual variation in the summer monsoon rainfall during the El Nino Southern Oscillation (ENSO) phases, that is, El Nino and La Nina throughout the Indian subcontinent and its subregions during 1986–2010. The analysis includes the performance assessments of the regional climate model (RegCM4) in simulating Indian summer monsoon rainfall through comparison with India Meteorological Department rainfall data. Observation clearly demonstrates that the El Nino/La Nina produced weaker/strong monsoon rainfall over India and it increases the interannual variability of the southwest monsoon. The capability and skill of RegCM4's Grell and Mix99 cumulus parameterization scheme in simulating Indian summer monsoon rainfall associated with extreme climate are usually higher in "dry" conditions rather below average for the accurate simulation of "wet" conditions. Also, model performance was good in defining the characteristics, spatial distribution, and trend of a dry spell during ENSO phases with observation. The model-simulated spatial and temporal value of wet spell during ENSO produces overestimated value over all India.

Plain Language Summary This study has been performed with the motivation of understanding the southwest monsoon drought/flood characteristics associated with El Nino and La Nina events. Climate change variability studies are of utmost importance for the planning of agriculture and economic policy. With this motivation, an attempt has been made to study the distinguishing features of Indian summer monsoon rainfall during El Nino and La Nina years over the Indian subcontinents and its subregions with Regional Climate Model (RegCM4). The finding of our study highlights the capability and skill of RegCM4's Grell cumulus parameterization scheme in simulating Indian summer monsoon associated with extreme climate are usually higher in "dry" condition rather below average for the accurate simulation of "wet" condition. The index of maximum count of consecutive dry days and consecutive wet days helps in accessing the deficient/excess rainfall over a regionalized and localized area.

1. Introduction

The southwest monsoon (SWM) is the world's most important monsoon system that affects nearly one third of the world population. The SWM maintains a periodicity annually in which more than 80% of the annual precipitation occurs during June–September and represents significant spatial and temporal variation which is dependent upon climatic and topographical features of the Indian subcontinent. The spatial and temporal interannual variability of Indian summer monsoon rainfall (ISMR) leads to large-scale drought and flood, resulting in a major effect on agriculture and the economy of the country (Guhathakurta & Rajeevan, 2006; Naidu et al., 2015; Parthasarathy et al., 1994; Turner & Annamalai, 2012). The strong influence of the Tropical Ocean on the variability of ISMR has been studied and epitomized by the El Nino Southern Oscillation (ENSO) phenomena (Shukla, 1987; Sikka, 1980; Webster & Yang, 1992). ENSO is a phenomenon of coupled ocean–atmosphere used to explain unusual climatic and weather patterns and also disrupt the ecosystem, agriculture, tropical cyclone, drought and flood, and other extreme weather events across the globe. The large-scale ocean–atmosphere climate interaction is linked to the periodic warming in the sea surface temperature (SST) across central and east equatorial Pacific Ocean termed as El Nino. On the other hand, La Nina (a cold event) represents

a period of below average SST across east central equatorial Pacific. Extreme El Nino severely disrupts global weather patterns affecting the ecosystem, agriculture, tropical cyclone, drought and flood, and other extreme weather events worldwide. It is well known that ENSO plays a prominent mode on the interannual scale to modulate the rainfall variability which influences the dry and wet conditions over the Indian subcontinent (Sahai et al., 2003). Initially, the association of El Nino and failures of ISMR was highlighted by Sikka (1980). Many studies have established that the El Nino/La Nina events are generally associated with dry (warm)/wet (cold) phase of the SWM (Ashok et al., 2004; Kripalani & Kulkarni, 2001; Walker, 1925). The study of Rajeevan et al. (2012) explained the association in the interannual variability of northeast monsoon over south peninsular India which is significantly linked with the phases and strengthening of ENSO and the Indian Ocean Dipole (IOD). Further, Sanap et al. (2019) explained the occurrence of heavy rainfall during El Nino phase and is weaker during La Nina and neutral phase in northeast monsoon. In recent decades, relationship between ISMR and ENSO weakened (C. P. Chang et al., 2001; Kumar et al., 1999). Previously, the weakening variability of ISMR and ENSO explained with the modulation of Indian Ocean dipole (IOD) (Ashok et al., 2004; Saji et al., 1999; Yang et al., 2007) and amplification of North Atlantic Oscillation (NAO) (Chang et al., 2001). Also, Cai et al. (2014) explained the occurrence of frequent cases of El Nino and La Nina after 2003 which is a result of the increased frequency of atmospheric convection in the eastern equatorial region due to the response of global warming. Therefore, in the global warming scenario, it is indeed important to examine how the ENSO–monsoon relationship changes in future climate and to understand the possible changes in the predictability of monsoon rainfall.

The Global Climate Models (GCMs) and Regional Climate Models (RCMs) can be used to simulate climate information about past, present, and future climate conditions. The coarse resolution of GCM which is hundreds of kilometers can cause inadequate simulation to epitomize the regional/local topographic features and mesoscale weather phenomena. Previous studies have shown that GCMs were not able to capture accurate and seamless simulation of the complex SWM system, due to the coarse resolution (X. J. Gao et al., 2001; Kripalani et al., 2007; Sabin et al., 2013). The existing state-of-the-art GCMs still have difficulties in simulating the subseasonal variability associated with Asian summer monsoon (Lin et al., 2008) and still this is a challenging to accurately simulate the interannual and intraseasonal climatological mechanism and phenomena such as, Madden–Julian oscillation and convectively coupled equatorial wave (Hung et al., 2013; Lin et al., 2006) in climate model.

Whereas, the dynamical downscale approach of RCM can improve the horizontal resolution (finer resolution) and able to simulate more detailed climate information about its physical processes and atmospheric dynamics (Giorgi, 2019; Giorgi et al., 2012). In this study, *state-of-the-art* RegCM (version 4) has been used to dynamically downscale the summer monsoon system over the South Asian Coordinated Regional Climate Downscaling Experiment (SA CORDEX) domain (Bhatla et al., 2016, 2018; Bhatla, Mandal, et al., 2019). The RegCM developed by the Earth System Physics group of the Abdus Salam International Center for Theoretical Physics (ICTP), Italy, has been widely used for simulating the past and future monsoon climatic system over the globe in the last 2 decades (N. Davis et al., 2009; X. Gao et al., 2012; Giorgi et al., 2012; Huang et al., 2013; Pal et al., 2007; Sylla et al., 2013). Previously, a large set of sensitivity experiments have been conducted using different cumulus parameterization schemes (CPSs), horizontal resolution, selection of domain, and effect of different land surface schemes to validating and verifying the RegCM simulation to understand the interannual and intraseasonal variability of SWM over India (Ashfaq et al., 2009; Bhatla et al., 2016, 2020; Dash et al., 2006, 2015; Ghosh et al., 2019; Nayak et al., 2019; Raju et al., 2015; Ratnam et al., 2009; Sinha et al., 2013). It is indeed important for RCM to understand the impact and severity of extreme climate association with modulator ENSO and IOD. The capability of RCM in representing the relationship between ENSO and rainfall has been performed over various regions of the South America (Da Rocha et al., 2014; Seth et al., 2007). Arini et al. (2015) state that the RegCM4 can explain rainfall type, the rainfall characteristics during ENSO over Kalimantan, Indonesia, which is characterized by deficient/excess rainfall El Nino/La Nina. However, the RCM capability in simulating the link between model and observation during ENSO is not competent (Ratnam et al., 2013). The study of Aldrian et al. (2007) depicts that to simulate/forecast the ENSO related rainfall anomalies, the model skill is higher in the dry season than

Table 1
Model (RegCM4.3) Configuration Used in the Study

Resolution	50 km horizontal	
Map projection	ROTMER	
Vertical level	18 sigma vertical levels	
Physics parametrization	Scheme/model	Reference
Radiation scheme	Community Climate Model version 3 (CCM3)	Kiehl et al. (1996)
Land surface model	Biosphere–Atmosphere Transfer Scheme (BATS Ie)	Dickinson et al. (1993)
Planetary boundary layer	Modified Holtslag	Holtslag et al. (1990); Holtslag and Boville (1993)
Convective Precipitation Schemes	(1) Modified-Kuo scheme (2) Grell scheme (3) MIT-Emanuel scheme (4) Tiedtke	Anthes (1977); Grell (1993); Emanuel (1991); Tiedtke (1989)
Large-Scale Precipitation Scheme	Subgrid explicit moisture scheme (SUBEX)	Pal et al. (2000)
Ocean surface flux scheme	Zeng's scheme	Zeng et al. (1998)

the rainy season. Thus, it is noteworthy to evaluate the performance assessments of the RCM dynamical downscale output to understand the association of ENSO with climate extreme at the regional and local scale.

The understanding of the SWM drought/flood characteristics associated with El Nino and La Nina events is of utmost importance for the planning agriculture and economic policy (M. Davis, 2001; Selvaraju, 2003). With this motivation, an attempt has been made to study the distinguishing features of ISMR during El Nino and La Nina years over the Indian subcontinents and its subregions. Also, the performance assessments of RegCM4's different CPSs have been done to simulating ISMR over India and its subregions during El Nino and La Nina events. The structure of the paper is as follows. The model descriptions are briefly described in Section 2. Section 3 described the data used in the study along with the methodology. In Section 4, detailed analysis has been explained, while Section 5 draws the paper together with conclusions.

2. Model Description

The stable version 4.0 of the Abdus Salam ICTP's RegCM4.3 has been used in this study. The *state-of-the-art* in the RCM RegCM has contributed significantly to the scientific society toward the study of climate change and its variability (Giorgi, 2006; Giorgi et al., 2012). To validate the model performance during El Nino and La Nina events, 25 years simulation with perfect lateral boundary condition of ECMWF's ERA-Interim reanalysis (Simmons, 2006) and NOAA's Weekly Optimum Interpolation SST (Reynolds et al., 2007) was conducted for the period of 1986–2010. The SA CORDEX domain (22°S–50°N; 10°E–130°E) has been selected as model domain with 50 km horizontal resolution with 18 sigma vertical levels. The RegCM4 is a hydrostatic limited area model, compressible, sigma-p vertical coordinate model with Arakawa B-grid system. The model implemented the Holtslag scheme (Holtslag et al., 1990) as planetary boundary layer schemes which is based on a nonlocal diffusion concept that takes into account countergradient fluxes in an unstable, well-mixed atmosphere. The radiation scheme is NCAR's Community Climate Model version 3 (CCM3); land surface parameterization given by Biosphere–Atmosphere Transfer Scheme (BATS Ie). The Subgrid explicit moisture scheme (SUBEX) is used for the large-scale precipitation scheme (Pal et al., 2000). The RegCM4 has four mainly available CPSs are, Grell scheme (Grell, 1993) with closure assumption of the Arakawa and Schubert, MIT (Emanuel, 1991), Kuo (Anthes, 1977), and Tiedtke (1989) and two mixed convection scheme (Emanuel

Table 2
List of Onset Year of El Nino, La Nina, and Neutral Year

El Nino	La Nina	Neutral
1986[a]	1988[b]	1989
1987[b]	1995	1990
1991[b]	1998[b]	1992
1994[a]	1999[b]	1993
1997[c]	2000	1996
2002[a]	2005	2001
2004	2007[b]	2003
2006	2008	
2009[a]	2010[b]	

[a]Moderate. [b]Strong. [c]Very strong.

over land; Grell over ocean [Mix98] and Emanuel over ocean; Grell over land [Mix99]) mentioned in Table 1.

3. Data Description and Methodology

For the performance assessment of the RegCM4, the model-simulated climate data compared with observation data of India Meteorological Department (IMD), which provided daily gridded rainfall data set (IMD4) at a high spatial resolution (0.25° × 0.25°) (Pai et al., 2014) for a period from 1986 to 2010. The rainfall data over the Indian subcontinent (6.5°N–37.5°N; 66.5°E–101.5°E) were considered for interpolating to gridded rainfall data (Rajeevan & Bhate, 2009). In this study, daily and monthly rainfall data are analyzed for the Indian summer monsoon period (June–September).

The El Nino years were identified based on the June–September average SST anomaly over the Nino3.4 region. The identification of ENSO years and climatology distribution of rainfall based on Nino3.4 SST anomaly index (5°S–5°N, 120°–170°W) during Northern Hemispheric summer (June–September: JJAS) 1986–2010. As per the definition, El Nino refers to a situation where five consecutive 3 months moving average Oceanic Nino Index Average (ONIA) values above 0.5 °C, whereas for the La Nina condition the ONIA value is below −0.5 °C (Table 2). The drought and flood year and its association with El Nino and La Nina were identified based on the percentage departure of ISMR anomalies. A year is defined as a drought/flood year when the standardized departure (SD) is less/more than −1 or +1, respectively. For the climate modeling perspective, a high-resolution dynamical downscaling with the resolution was set up in RegCM4 over the SA CORDEX domain. The simulation of ENSO events using six convection schemes of RegCM4.3 has been done during the period of 1986–2010. The interannual variability of rainfall associated with El Nino and La Nina is stud-

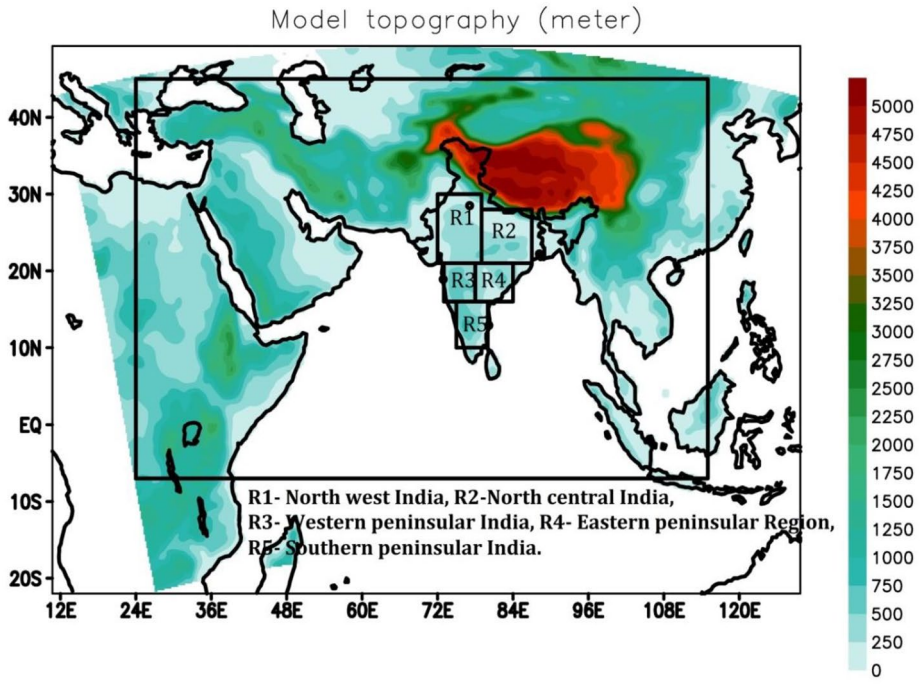

Figure 1. Model domain and topography (in meter) consider for the study. Black rectangular box denotes South Asian CORDEX domain (22°S–50°N; 10°E–130°E) and R1, R2, R3, R4, and R5 are the domain for the five subregions of India, namely, *Northwest India*, *Northcentral India*, *Western Peninsular India*, *Eastern Peninsular India*, and *Southern Peninsular India*, respectively. CORDEX, Coordinated Regional Climate Downscaling Experiment.

ied by comparing observed gridded rainfall data set of IMD over India and its subregions as *Northwest India (R1)*, *Northcentral India (R2)*, *Western peninsular India (R3)*, *Eastern peninsular India (R4)*, and *Southern peninsular India (R5)* (Figure 1) (Bhatla et al., 2019). The selection of best fit model CPS has been done *Skill Score* (Zou et al., 2014). The least values of skill score signify the best fit CPS for model simulation for El Nino and La Nina years:

$$\text{skill score} = \log\left[\frac{\left(4\left(\frac{\sigma_o}{\sigma_m}+\frac{\sigma_m}{\sigma_o}\right)^2\right)}{(1+r)^4}\right]$$

where σ_o and σ_m are standard deviations of observation and model simulation, respectively, and r is the correlation coefficient between them.

Thereafter, consecutive dry days (CDDs) (below 1 mm rainfall) and consecutive wet days (CWDs) (more than 1 mm rainfall) are calculated and used in the result analysis during El Nino and La Nina over five selected subregions of India. The CDD, defined as the maximum number of CDDs with daily precipitation below 1 mm. And, the CWD define as the maximum number of wet days with daily precipitation equal to or more than 1 mm.

4. Results and Discussion

4.1. Regional Characteristics of Summer Monsoon Rainfall Patterns in India and Their Relations With Nino3.4 SST Anomaly

The time series of ISMR which is expressed as SD of seasonal (JJAS) summer monsoon rainfall from the normal has been analyzed with Nino3.4 SST anomaly (Figures 2a–2f). The strongest negative correlation coefficient has been obtained, that is, −0.51 in between the standardized all India summer monsoon (AISMR) and Nino3.4 SST anomaly for the period 1986–2010. During the climatological period of 1986–2010, years 1986, 1987, 1991, 1994, 1997, 2002, 2004, 2006, and 2009 are categorized as onset El Nino years based on positive ONI (above 0.5°C). On the other hand, the negative ONI (below −0.5°C) declared the La Nina years such as 1988, 1995, 1998–2000, 2005, 2007, 2008, and 2010. The strength of El Nino and La Nina events has been mentioned in Table 2. From the observed AISMR association with Nino3.4 SST, it has been observed that the frequent cases of El Nino and La Nina have occurred after 2003. This finding has been related to the response of global warming, thus, the increased frequency of atmospheric convection in the eastern equatorial region has been observed (Cai et al., 2014), so that frequent cases of El Nino and La Nina have occurred. The time series of standardized rainfall also explains the flood (greater than 1 SD) and drought years (less than 1 SD) which are associated with the occurrence of El Nino and La Nina years. During this period, all the five drought years (1986, 1987, 2002, 2004, and 2009) in India are coincide with El Nino years, that is, 5 out of 9 years (55%) which supported by the study Kripalani and Kulkarni (1997) that is most of the droughts are connected with El Nino episodes. The phenomena of drought could be explained by the finding of Kripalani et al. (1996), the positive SST anomaly for five consecutive 3 months average trigger the enhancement of anomalous tropical convection across the central and eastern equatorial Pacific and suppressed/inhibit the convection over the western Pacific. On the other hand, the major flood condition over India are, that is, 1988, 1994, 2005, 2006, and 2007 (33%) in which three major flood years are associated with the La Nina years, that is, 1988, 2005, and 2007 except 1994 and 2006 which are moderate and weak El Nino years (Table 3). So it a fact that the association of significant Dipole Mode Index (DMI) suppresses the effect of El Nino year (1994) (Saji et al., 1999) and causes the flood-like condition over India mainly over Northwest, Northcentral, and Western peninsular India. A significant year to year variability of AISMR has been observed in Figure 2a. The strong inverse relationship of AISMR with Nino3.4 ONI Index has been observed during 1987 (strong El Nino), 1988 (strong La Nina), 1997 (very strong El Nino), 2002 (moderate El Nino), and 2009 (moderate El Nino) for AISMR. In Figures 2b–2f, relationship of Nino3.4 SST anomaly has been studied with the observed summer monsoon rainfall over important five subregion of India, that is, R1–R5. The climatology and topography of these subregions are unique in nature. So that the distribution summer monsoon rainfall is not evenly over these regions. In the R1 region, AISMR correlation

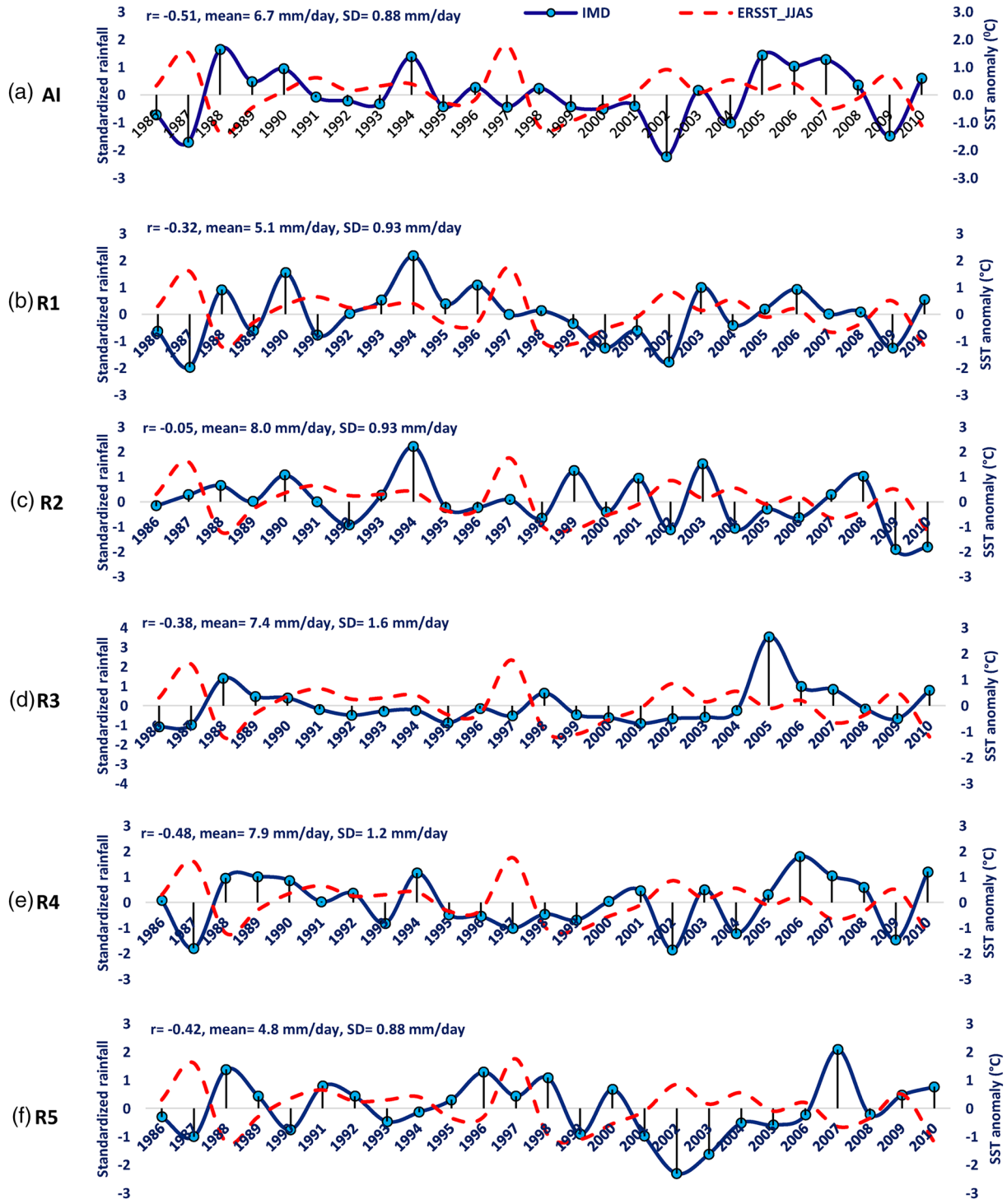

Figure 2. (a–f) The time series of Indian summer monsoon rainfall (expressed as the departure of seasonal summer monsoon rainfall from the normal)—(a) for all India region: AI, (b) for *Northwest India*: R1, (c) for *Northcentral India*: R2, (d) for *Western Peninsular India*: R3, (e) for *Eastern Peninsular India*: R4, and (f) for *Southern Peninsular India*: R5 with Nino3.4 SST anomaly (1986–2010).

with the Nino3.4 SST is the −0.32 that means the inverse correlation is moderate in the nature. The drought year for the Northwest region is 1987, 2000, 2002, and 2009 which are strongly associated with the El Nino years (Figure 2b). Two major flood years have been identified over the R1 region, that is, 1990 and 1994 neutral year and El Nino year, respectively. The interpretation of 25-year climatology indicated that the

Table 3
Association of Drought and Flood With El Nino and La Nina Years for All India and Its Subregions

	Drought	Flood
All India	*1986*, *1987*, *2002*, *2004*, *2009*	**1988**, *1994*, **2005**, *2006*, **2007**
R1	*1987*, *2000*, *2002*, *2009*	***1990*** , *1994*
R2	*2002*, *2004*, *2009*, **2010**	*1994*, **1999**, ***2003***
R3	*1986*, *1987*	**1988**, **2005**
R4	*1987*, *2002*, *2004*, *2009*	*1994*, *2006*, **2010**
R5	*2002*, ***2003***	**1988**, ***1996***, **2007**

Note. Performance of RegCM4 for dynamically downscaling of El Nino/La Nina events during southwest monsoon over India and its regions. Italic: associated with El Nino years; Bold: associated with La Nina years; Bold & Italic: associated with neutral years.

frequency of drought is more in the North West region in comparison to the flood. Also, the effect of La Nina did not cause effective flooding in this region. The most important region for agrarian purposes in the Northcentral India (R2), this region includes the Indo Gangetic basin. Hence, the purpose of the study to analyze the effect of ENSO over ISMR is most important for this region. The selected El Nino years cause major drought such as 2002, 2004, and 2009 along with the year of 2010 (La Nina) (Figure 2c). The year of 2010 was a strong La Nina years but this effect did not bring flood/wet conditions all over India. Against the nature of La Nina year, Northcentral India faces a drought-like condition during 2010. The flood years for region R2 are 1994 (El Nino), 1999 (La Nina), and 2003 (neutral). This analysis shows that the probability of drought is predictable on the basis of its association with the El Nino event. On the other hand, it is quite difficult to assume a flood condition based on the occurrence of La Nina events. As per the record of the natural disastrous events, floods are the most dangerous, frequent, and widespread events throughout the world according to the World Meteorological Organization (2013). The region of Western peninsular shows a strong association of ISMR with the Nino3.4 index as the strong El Nino years caused the deficient rainfall, on the other hand strong La Nina also associated with the flood years over this region (Figure 2d). The extreme precipitation event of 2005 has been noticed over the western peninsular, which is localized over Mumbai (94.4 cm in 24 h), Maharashtra on July 26, 2005 (H. I. Chang et al., 2009). The example of the 2005 Mumbai rainfall causes an immediate effect on the population and economy of the country. Thus, the regionalized pattern of ENSO association with the dry and wet year of ISMR also is considered for the study. Eastern peninsular India is showing the highest correlation coefficient with Nino-3.4 ONI, that is, −0.48. That means the inverse relationship of ENSO and ISMR directly impacts the rainfall distribution over this region (Figure 2e). Part of Western, Eastern peninsular India, and Northcentral India receive rainfall largely from the SWM from June to September; hence, these regions are more susceptible to the interannual and intraseasonal rainfall variability. Jones et al. (1986) suggested that the changes in rainfall and arid area were a consequence of the spatial changes in Indian summer monsoon circulation characterized by the strengthening of the Arabian Sea branch and weakening of the Bay of Bengal branch. The anomalous increase in the SST index (ONI) indicted the extreme dry/drought year, that is, 1987, 1997, 2002, and 2009 in the region. Despite the moderate and weak El Nino, that is, 1994 and 2006, the R4 region received excess SWM rainfall from the normal due to the association of positive DMI. So the changing SST over the Pacific Ocean and the Indian Ocean eventually linked to the strengthening/weakening of the two important branches of SWM. During the strong La Nina year, that is, 2010, its major effects have been observed over the R4 region but the same year also bring drought-like condition over the R2 region (Figures 2c and 2e). Hence, it could be predicted that the occurrences of regionalized excess and deficient rainfall had a unique relationship with the modulation of the teleconnection phenomena such as El Nino and La Nina. The lowermost peninsular region, that is, southern peninsular region receives plenty of summer monsoon rainfall during the onset of monsoon due to orography of the Western Ghats. The major dry year are observed during 2002 and 2003 (Figure 2f). The year 2002 was the moderate El Nino but it gets intensify and majorly affects the R1, R3, and R5 regions. The association of ISMR over the R5 region and Nino3.4 (ONI) SST shows that the negative anomalous increase is often associated with the excess rainfall year, that is, 1988 and 2007. One neutral year (1996) also causes the flood-like condition over the R5 region. The frequent and increasing number of heavy and extreme rainfall events can be explained by a various number of possible mechanisms, namely, westward shifting of rainfall, aerosol effect, land use change, SST changes, and global changes (Roxy et al., 2015). Overall, among 25 years of climatological period, ISMR was associated with 18 ENSO events which are about 72% of the cases associated with the Pacific Ocean influence.

4.2. Spatial Distribution of ISMR During El Nino and La Nina

The spatial distribution of average SWM rainfall during El Nino years, that is, 1986, 1987, 1991, 1994, 1997, 2002, 2004, 2006, and 2009 are delineated in Figure 3. The observed (IMD) monsoon rainfall spatial distri-

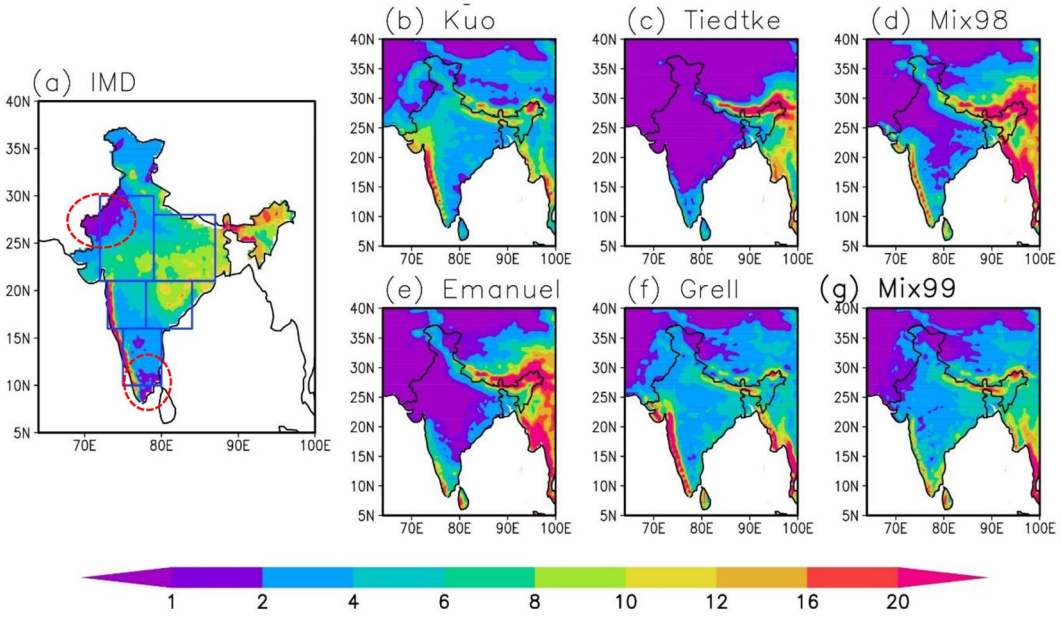

Figure 3. (a–g) Average all Indian summer rainfall distribution during El Nino years obtained from (a) IMD gridded data set, red circle showing the major rain deficient area during El Nino years, and compared with the simulation of six different convection schemes of RegCM4: (b) Kuo, (c) Tiedtke, (d) Mix98, (e) Emanuel, (f) Grell, and (g) Mix99. In this figure, solid blue box represents the selected subregions over the Indian subcontinent, namely, *Northwest India: R1*; *Northcentral India:* R2; *West Peninsular India:* R3; *Eastern Peninsular India:* R4; and *Southern Peninsular India:* R5. IMD, India Meteorological Department.

bution and variability have been studied over India and its different subregions such as R1–R5 during El Nino years (Figure 3a). The observed rainfall pattern depicts two major rain deficient zones which are the northern part of the western region and the southern part of Eastern Ghats (denoted as a red dotted circle in Figure 3a). The decrease in the monsoon rainfall over the Indian region was supported by Turner and Annamalai (2012) and Varikoden et al. (2015) during the post-1950s. The frequent occurrence of ENSO events in the post-1990s might be a reason behind the decrease in monsoon rainfall. The association of ENSO is causing dry/wet monsoon during El Nino and la Nina, respectively. These regions received less than 2 mm/day average monsoon rainfall during El Nino years. The core monsoon region shows the average rainfall between 8 and 16 mm/day during El Nino events. The maximum average monsoon rainfall was received by western at and northeast regions, that is, more than 16 mm/day. The RCM (RegCM4) simulation for SWM rainfall using different CPSs, that is, Kuo, Tiedtke, Mix98, Emanuel, Grell, and Mix99 is compared with the observed data set of IMD rainfall during El Nino years (Figures 3a–3g). The monsoonal rainfall variability over the Indian subcontinent is well captured by Kuo, Grell, and Mix99 CPSs of RegCM4 against observed rainfall. The intensity rainfall over the core monsoon region and the northeast region is not captured by RegCM4. The model performance in simulating monsoon rainfall using Tiedtke and Emanuel CPSs is not up to confidence level to consider for further study.

Figures 4a–4g represent the SWM rainfall over the Indian subcontinent during nine La Nina events (1986–2010). The spatial distribution and variability of rainfall are analyzed with observed IMD rainfall (Figure 4a) and compared with the RegCM4-simulated rainfall over the Indian domain (Figures 4b–4g). During the La Nina years, India received a surplus amount of rainfall over Western Ghats (more than 20 mm/day), Northeast region (8–20 mm/day), central India (8–12 mm/day), and foothills of the Himalaya (8–12 mm/day). It could be analyzed that eastern peninsular India received the maximum average distribution of monsoon rainfall during La Nina as compared to the El Nino years. The climatology of summer monsoon rainfall over India during La Nina years reveals that a huge expanse of rainfall is located over the foothills of the Himalayas. Also, the foothills of the Himalayan including Indo Gangetic plain is experiencing the moderate to heavy monsoon rainfall, which is absent during the El Nino years. The above-mentioned two major drought-prone zones during El Nino years were missing during the La Nina years. That means the

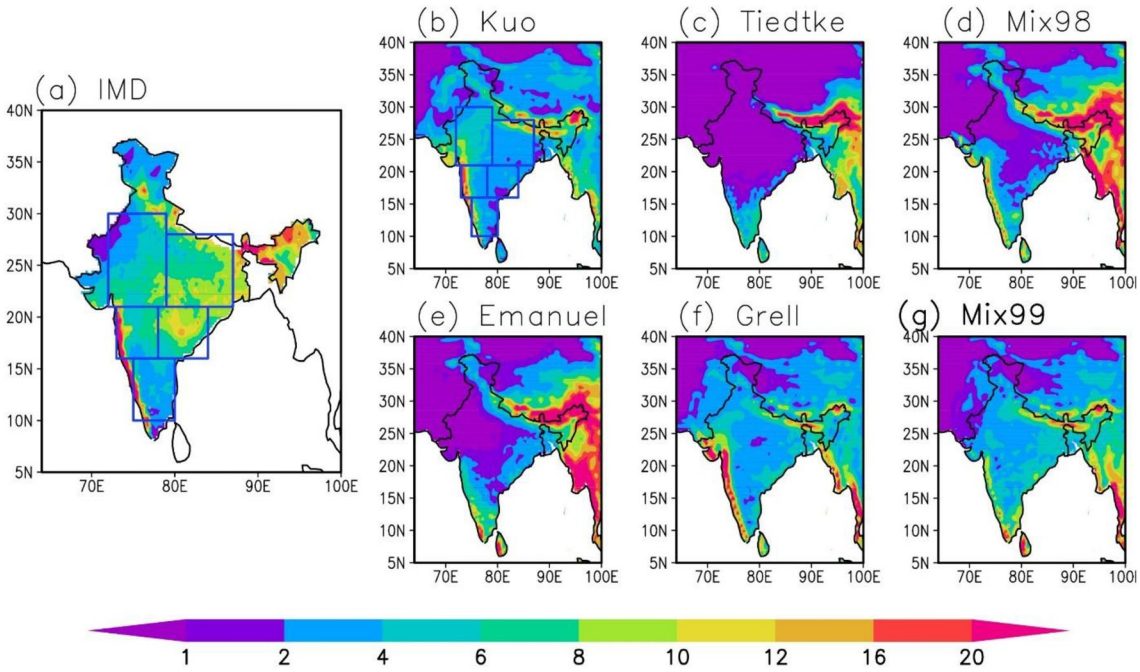

Figure 4. (a–g) Same as Figure 3, except for average all Indian summer monsoon rainfall distribution during La Nina.

teleconnection climatic condition brings the good monsoon rainfall over the drought-prone regions. The spatial variability of observed monsoon rainfall compared with the model-simulated rainfall during June–September. The model simulation composite plot consists of the six CPS simulation, that is, Kuo, Tiedtke, Mix98, Emanuel, Grell, and Mix99 which is showing the monsoon rainfall over the Indian subcontinent. Similar to the previous results, the Kuo-, Grell-, and Mix99-simulated monsoon rainfall are closer to the observed rainfall. All India mean monsoon climatology is well simulated by the model selected CPSs except over the core monsoon region. The Model capability is good in simulating the orographic rainfall over the Western Ghats except the central plateau region.

4.3. Percentage Rainfall Departure During El Nino and La Nina Years

The capabilities of the model to capture changes in the summer monsoon rainfall over the Indian subcontinent during two extreme cases El Nino and La Nina have been analyzed in terms of percentage rainfall departure from the normal (Figures 5 and 6), respectively. The above explanations prove that the Indian drought is mostly associated with the El Nino episode, the spatial distribution of rainfall departure during the El Nino events shows that its effect is more regionalized or localized in the observation data (Figure 5a). Two significant rainfall deficient zone (less than 20% rainfall from the normal) has been observed in the upper part northwest India (26°N–30°N; 72°E–80°E) and southern region (5°N–20°N; 75°E–80°E) of India. Also, some regions such as central India, lower Gangetic region, eastern peninsula, and Western Ghats have received more than the normal rainfall (more than 20% rainfall from the normal). Hence, the observed feature of monsoon rainfall departure during El Nino years has been compared with the model simulation, in which the Grell and Mix98 CPS simulations were closer to the observation. Otherwise, complex and advance CPSs such that Tiedtke and Emanuel show very large rainfall departure from the observation (i.e., less than 30%). In Figures 6a–6g, the Indian summer rainfall percentage departure from the normal has been plotted during La Nina years. The observed ISMR pattern during the La Nina episode shows a distinguished nature of excessive rainfall departure (in the range of 20–30; exactly opposite from the El Nino episode) in two regions which is the Himalaya region (26°N–35°N; 70°E–80°E) and southern region of India. In the western peninsular region (localized over Mumbai), excessive rainfall, that is, more than 50% from the normal rainfall has been observed during the La Nina episode. On the other hand, central India was received less than average/normal rainfall during the La Nina years (1986–2010). The RegCM4's CPSs

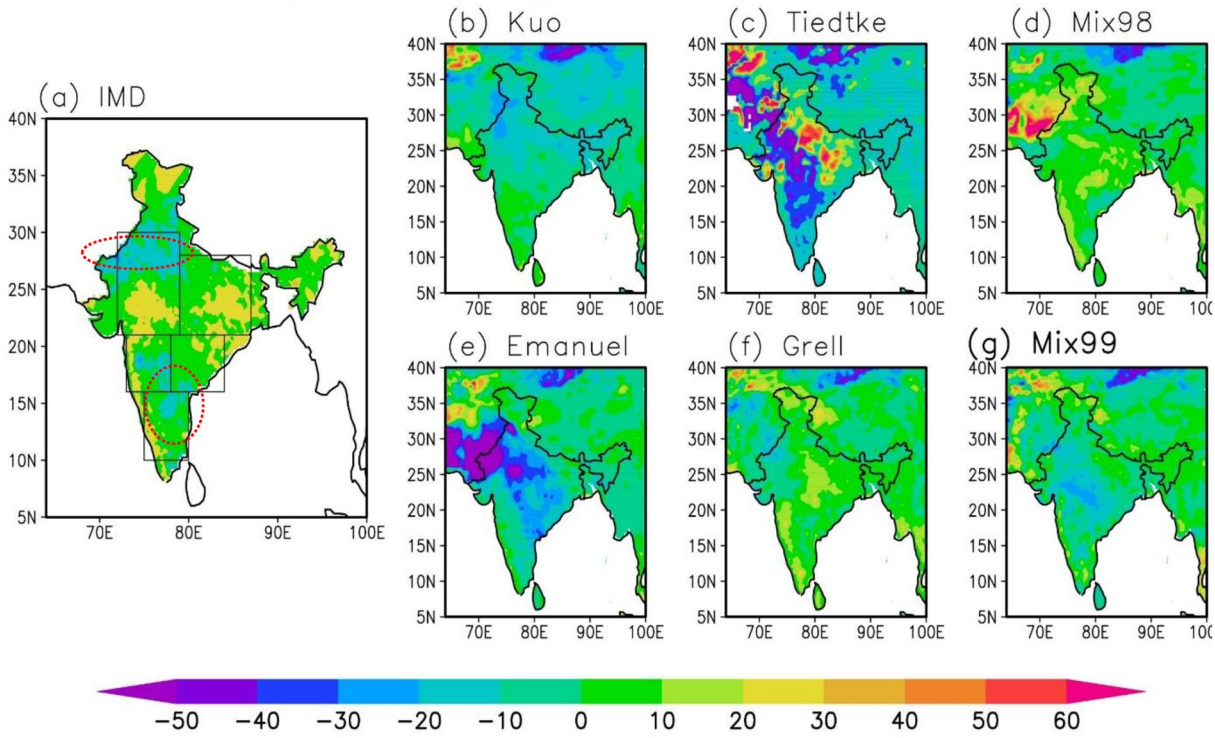

Figure 5. (a–g) Same as Figure 3, except for percentage summer monsoon rainfall departure from accumulated ISMR during El Nino years. ISMR, Indian summer monsoon rainfall.

(Mix98 and Mix99) were able to simulate some of the distinguishing features of ISMR departure during the La Nina (Figures 6b–6g). The CPSs Kuo and Grell were showing the negative ISMR departure than normal, on the other hand the Emanuel and Tiedtke show the excessive rainfall departure from the normal. Thus, the observation and model simulation proves that the El Nino/La Nina produced weaker/strong monsoon

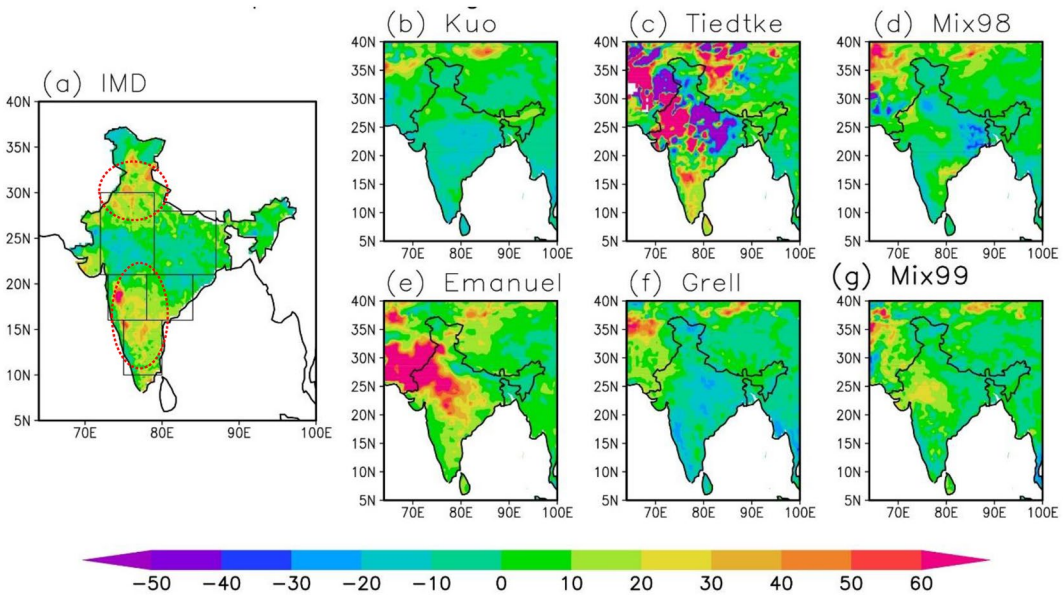

Figure 6. (a–g) Same as Figure 3, except for percentage summer monsoon rainfall departure from accumulated ISMR during La Nina years. ISMR, Indian summer monsoon rainfall.

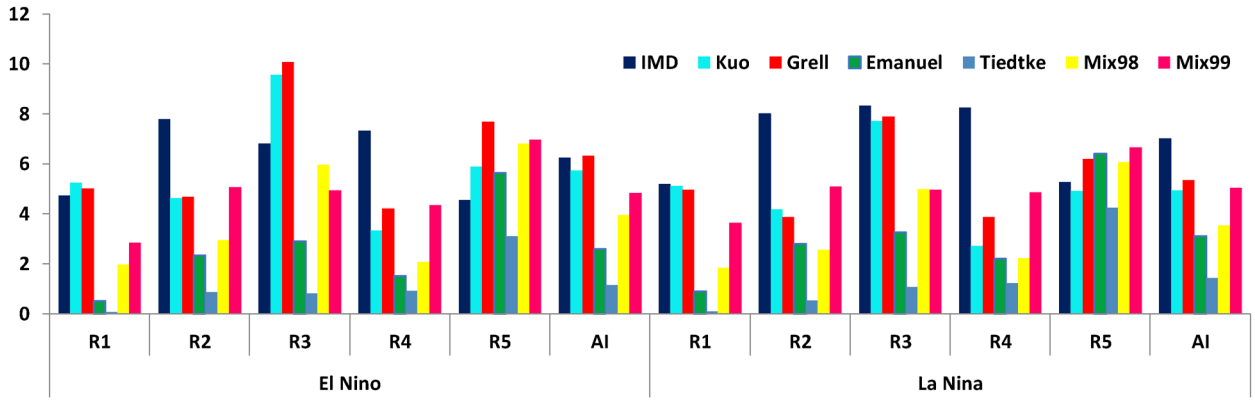

Figure 7. Average summer monsoon rainfall of IMD data and cumulus convection schemes during El Nino and La Nina year over India and its subregions. IMD, India Meteorological Department.

over India and its subregions which may induce or accelerate the intraseasonal and interannual variability of the SWM rainfall.

The above analysis shows that the model simulation of ISMR during El Nino and La Nina episode is sensitive to the selection of CPSs. The Grell scheme efficiently improve the performance because of the triggering mechanism (the lifted parcel attains moist convection) and no direct mixing occurs between the cloudy air and the environment air except at the top and bottom of the circulations (Grell, 1993). That is why the Grell and Mix99 are best CPSs to represent spatial and temporal variability of the ISMR during El Nino and La Nina period. On the other hand, the performance of complex scheme such as Emanuel and Tiedtke affected in the extreme condition (strong El Nino and La Nina) which involves the episodic and inhomogeneous mixing of cloud (Emanuel, 1991) and parameterizes the tropical deep convection (Bao et al., 2013), respectively, as the triggering mechanism processes in simulating the precipitation. The model-simulated average ISMRs over all India and different subregions were compared with the observation data of IMD for El Nino and La Nina year (Figure 7). In the El Nino and La Nina years, model's Grell CPSs simulation was closed to the observation for region R1 and all India. In the R2 and R4 regions, the model simulation is underestimated the actual rainfall. The model simulation over the southern peninsular was overpredicted by the Grell, Emanuel, Mix98, and Mix99 CPSs. Thus, it is difficult to select one single CPS to simulate perfect ISMR over India due to complex climatology and regionalized topographical differences. However, a unique skill score has been evaluated to access the performance of all model's CPS based on standard deviation and correlation coefficient between observation and model simulation (1986–2010) (Figure 8). The region-wise evaluation of skill score presents a comprehensive view of model skill in the seamless simulation of ISMR over the Indian subcontinent. Based on the least value of skill score, the Grell CPS is best in simulating the spatial, temporal, and correlation characteristics of observation during El Nino and La Nina. The maximum

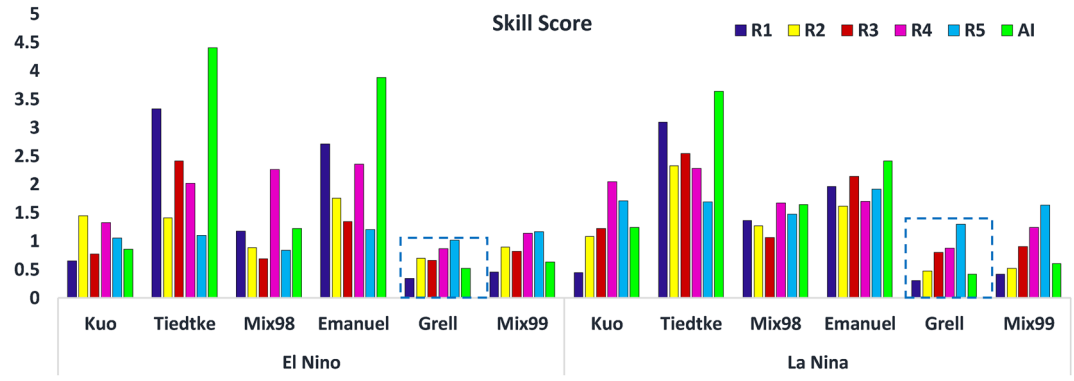

Figure 8. Schematic skill score of cumulus parameterized scheme of RegCM4 over the Indian subcontinent and its five subregions during El Nino and La Nina years, respectively.

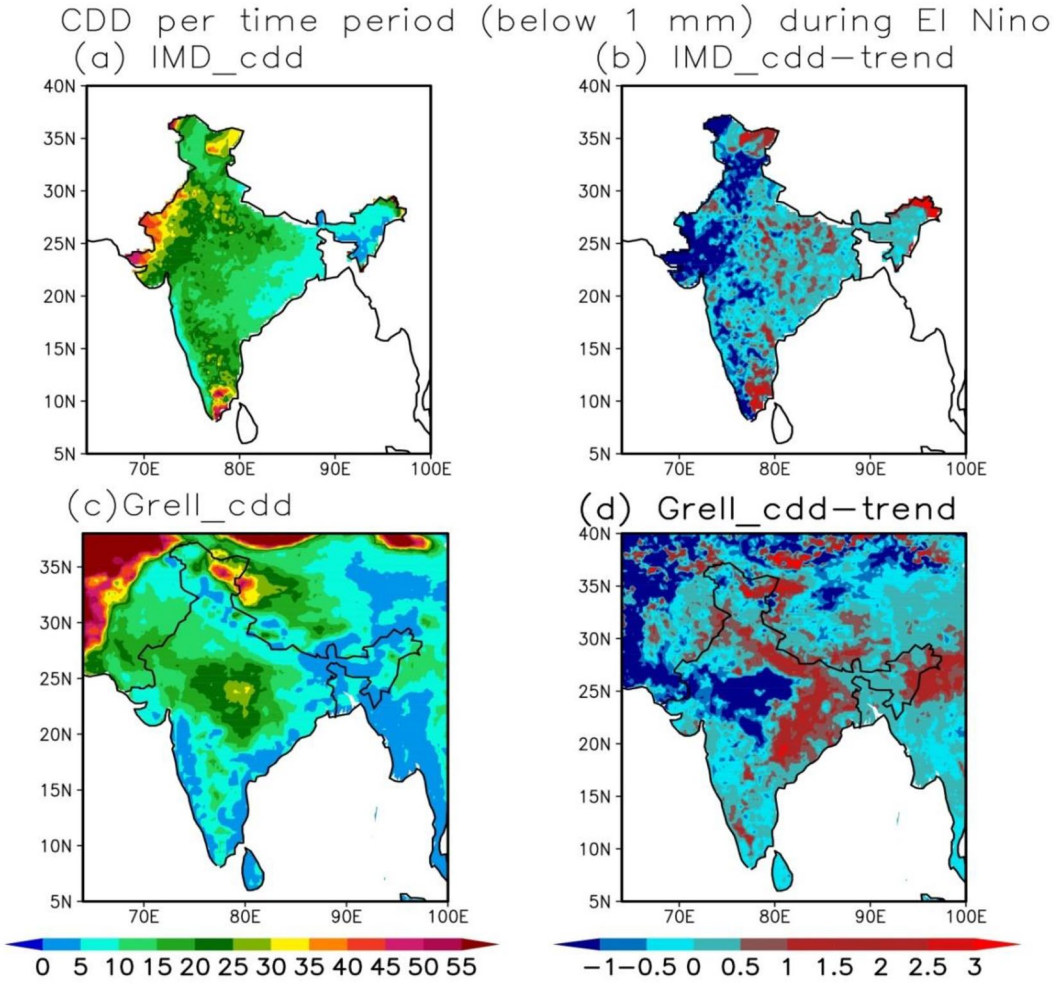

Figure 9. (a–d) Spatial plot for average consecutive dry days (below 1 mm) during ISMR. (a, b) CDD and its trend for observed rainfall data of IMD during El Nino years, respectively. (c and d) CDD and its trend for RegCM4's Grell CPS-simulated rainfall during El Nino years, respectively. ISMR, Indian summer monsoon rainfall; CDD, consecutive dry day; IMD, India Meteorological Department; CPS, cumulus parameterization scheme.

value of the Skill score was shown by the Emanuel and Tiedtke schemes over all subregions. The performance of Kuo and Mix99 CPSs is the second best and could be acceptable in terms of skill score. So that further analysis of characteristics dry spell and wet spell during the El Nino and La Nina has been done using RegCM4's Grell CPS and the observation data.

4.4. Defining the Characteristic, Spatial Distribution, and Trend of Dry Spell and Wet Spell During ENSO With Model and Observation

The spatial plot for average CDD (below 1 mm) during ISM and its trend for observation and RegCM4's Grell CPS have been analyze during El Nino (Figures 9a–9d) and La Nina years (Figures 10a–10d), respectively. The term maximum CDD is used as an index to assess the deficient rainfall or drought over a region (Field et al., 2012; Frich et al., 2002; Zhang et al., 2011). The observation data show that the spatial distribution of maximum average CDD (more than 50 CDD) over the eastern Himalaya, northwest region, and the Eastern Ghats of the southern peninsula (Figure 9a) during El Nino years. Also, CDD spatial trend is supplementary to show that its trend is increasing over eastern Himalaya, eastern Indo Gangetic plain (IGP), and Eastern Ghats of the southern peninsula and eastern peninsular part of India (more than 1 CDD/year). On the other hand, the maximum CDD over the Northwest region shows a decreasing trend of 1 CDD/year during El Nino years. The Grell CPS-simulated ISMR is showing the spatial distribution of maximum CDD

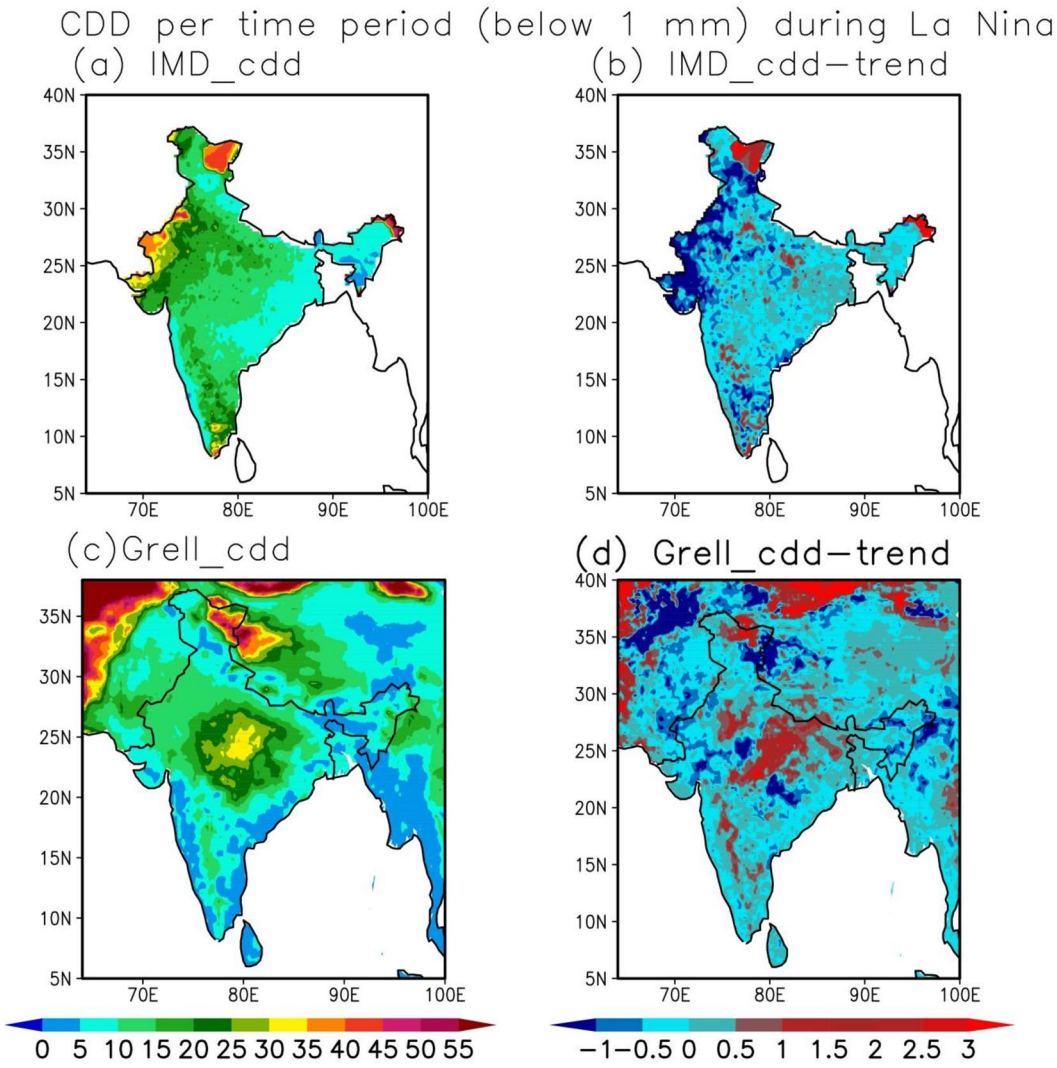

Figure 10. (a–d) Spatial plot for average consecutive dry days (below 1 mm) during ISMR. (a and b) CDD for observed rainfall data of IMD during La Nina, respectively. (c and d) CDD and its trend for RegCM4's Grell CPS-simulated rainfall during La Nina years, respectively. ISMR, Indian summer monsoon rainfall; CDD, consecutive dry day; IMD, India Meteorological Department; CPS, cumulus parameterization scheme.

over central India (30–35 CDD). During the La Nina years, the average CDD distribution is lesser than El Nino years over northwest India and southern India. The model performance is not up to mark to represent the spatial distribution of CDD over India. The model-simulated CDD during El Nino and La Nina is not evenly distributed as the observation but the temporally average distribution of CDD is well simulated by the Grell CPS (Figure 13a) with minimum error (Figure 10).

The average wet spell has been calculated as the CWD (equal and above 1 mm) for ISMR during El Nino and La Nina, respectively (Figures 11a–11d and 12a–12d). The IMD data illustrate the spatial variability of CWD and its trend in Figures 11a and 11b. The maximum average CWD is located over the Western Ghats and northeast India, that is, above 40 CWD during El Nino years. Over central India, the CWD lies in between the range of 15–25. The spatial trend of El Nino CWD depicts an increasing trend over the Western Ghats region and Uttarakhand which is more than 3 CWD/year during El Nino years. Also, interesting features have been analyzed with the observation that is during El Nino trend of CWD was decreasing over upper northeast India (less than 2 CWD/year). The extent of the wet spell (CWD) and its trend has been increasing over the high rainfall region during ISM (La Nina), that is, over central India, Western Ghats, eastern Himalaya, and northeast India (Figures 12a and 12b). The model Grell CPS was overestimating the average CWD and

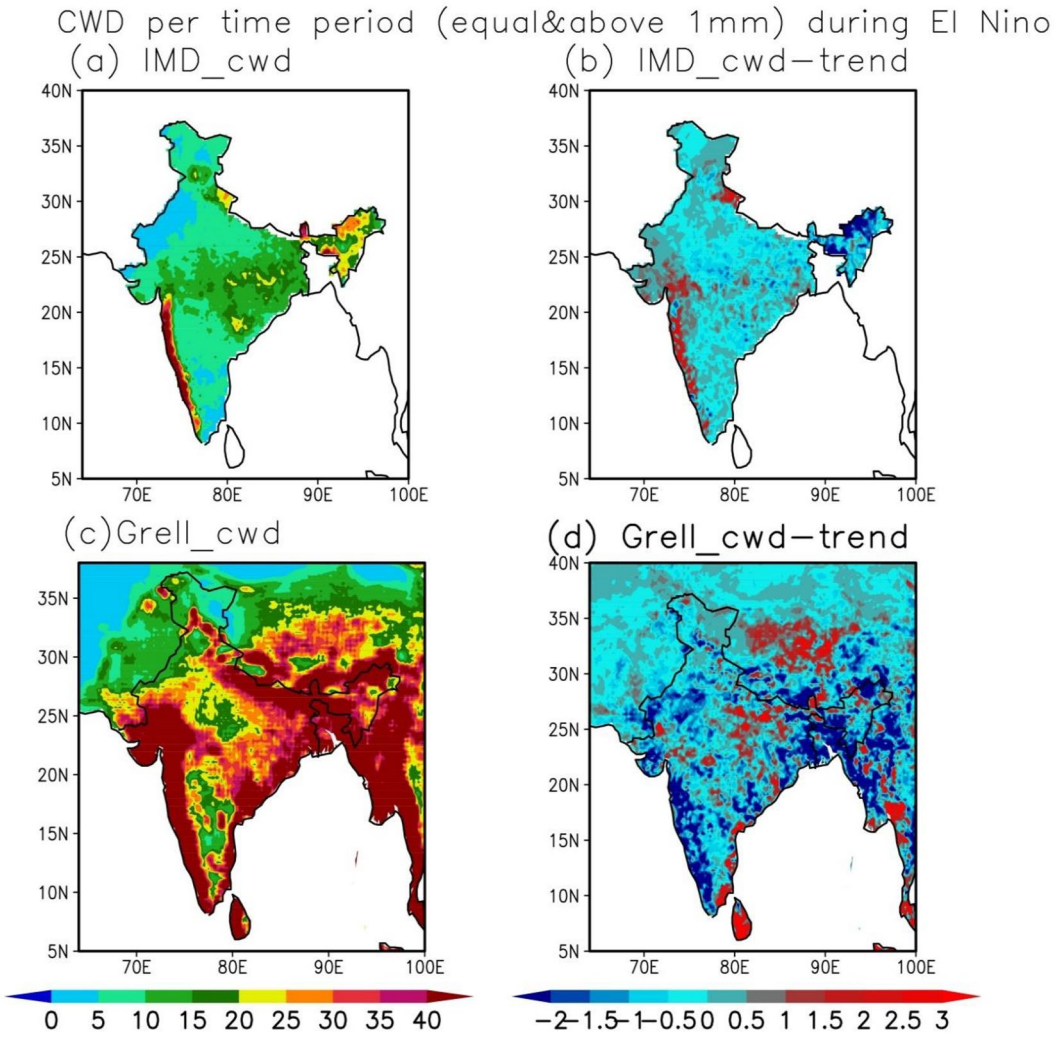

Figure 11. (a–d) Spatial plot for consecutive wet days (equal and above 1 mm) during ISMR. (a and b) CWD and its trend for observed rainfall data of IMD during El Nino, respectively. (c and d) CWD and its trend for RegCM4's Grell CPS-simulated rainfall during El Nino years, respectively. ISMR, Indian summer monsoon rainfall; CWD, consecutive wet day; IMD, India Meteorological Department; CPS, cumulus parameterization scheme.

its trend value over India and its subregions during ENSO events. Also, the temporal distribution of CWD over subregions of India is overestimating the value by 3 times the observation (Figure 13b). The study of Aldrian et al. (2007) depicts that to simulate/forecast the ENSO related rainfall anomalies, the model skill is higher in the dry season than the rainy season. That is why the wet spell simulated in the model is relatively higher than the observation. The application of systematic bias correction will help in the accurate simulation of the occurrence and frequency of wet spells in the RCM.

Comprehensively, it is an important factor to consider the spatial and temporal variability and trend of CDD and CWD for ISMR. This study of observational and model trends of CDD and CWD indicates that El Nino and La Nina episodes can modulate the probability of occurrences and length of wet spell and dry spell in such a way to produce weak or strong monsoon years over different subregions of India.

5. Conclusions

In this study, the interannual variation in the precipitation during the ENSO phases, that is, El Nino and La Nina throughout the Indian subcontinent and its subregions has been done. The consistent spatial and temporal modulation of monsoon precipitation has been observed with the help of IMD

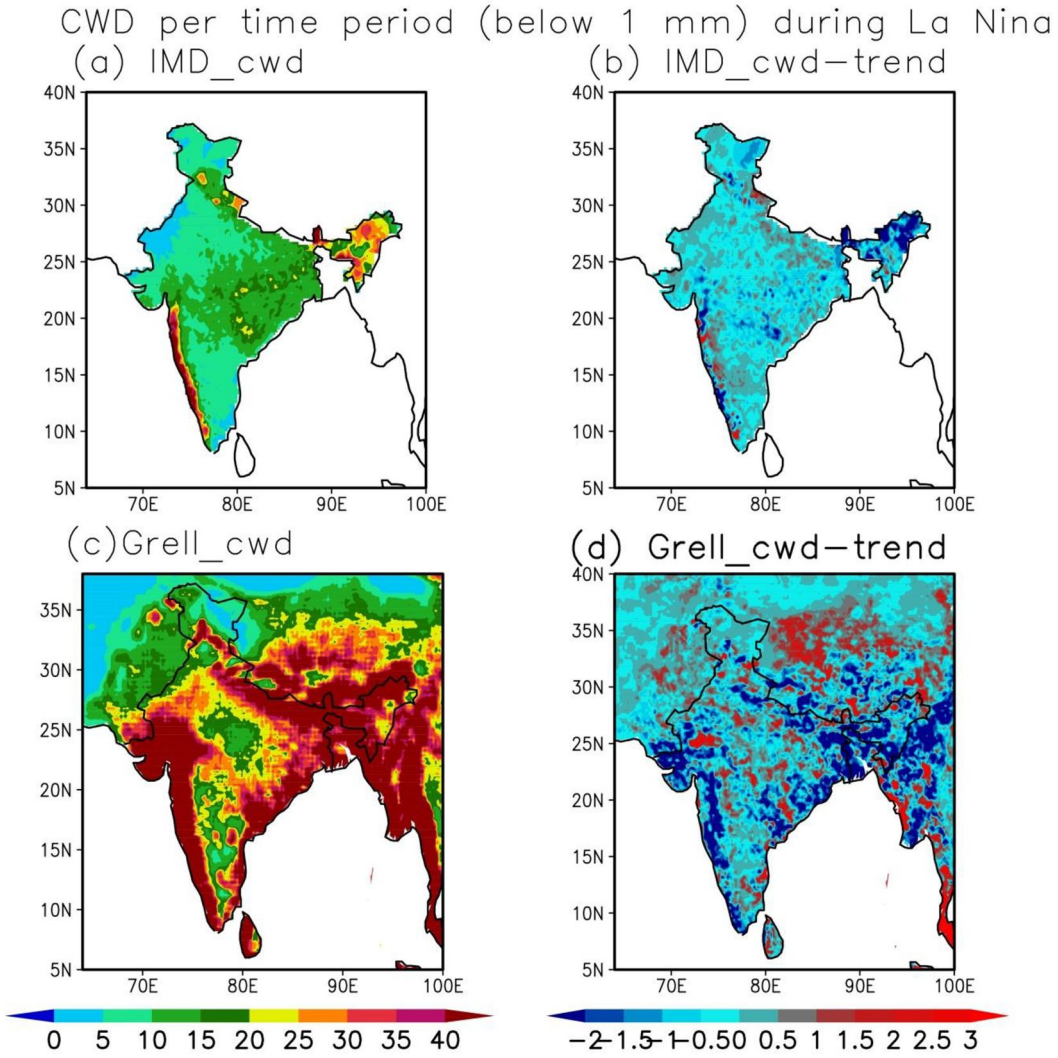

Figure 12. (a–d) Spatial plot for consecutive wet days (equal and above 1 mm) during ISMR. (a and b) Average CWD and its trend for observed rainfall data of IMD during La Nina, respectively. (c and d) CWD and its trend for RegCM4's Grell CPS-simulated rainfall during La Nina, respectively. ISMR, Indian summer monsoon rainfall; CWD, consecutive wet day; IMD, India Meteorological Department; CPS, cumulus parameterization scheme.

and model simulation which is significantly associated with the El Nino and will highly affect the regions of upper northwest India (26°N–30°N; 72°E–80°E), Eastern Ghats of the southern peninsular region (5°N–20°N; 75°E–80°E), and northeast India. On the other hand, during La Nina, ISMR departure from the mean rainfall was excess in the Himalaya region (26°N–35°N; 70°E–80°E), western peninsular region (localized over Mumbai; more than 50% from the normal rainfall), and southern region of India. This can be concluding as the frequent and prolong occurrences La Nina events will associate future flood-like conditions in the above-mentioned regions. The capability and skill of RegCM4's Grell and Mix99 CPS in simulating Indian summer monsoon associated with extreme climate are usually higher in "dry" condition rather below average for the accurate simulation of "wet" condition. The spatial and temporal representations of CDD and CWD signify deficient/excess rainfall which is regionalized phenomena modulating occurrence/frequency of climate extreme over India. In the global warming scenario, the finding of this study highlights the importance of the selection of RCM to understand the potential impact and severity of extreme climate changes to understand the possible changes in the predictability of SWM rainfall.

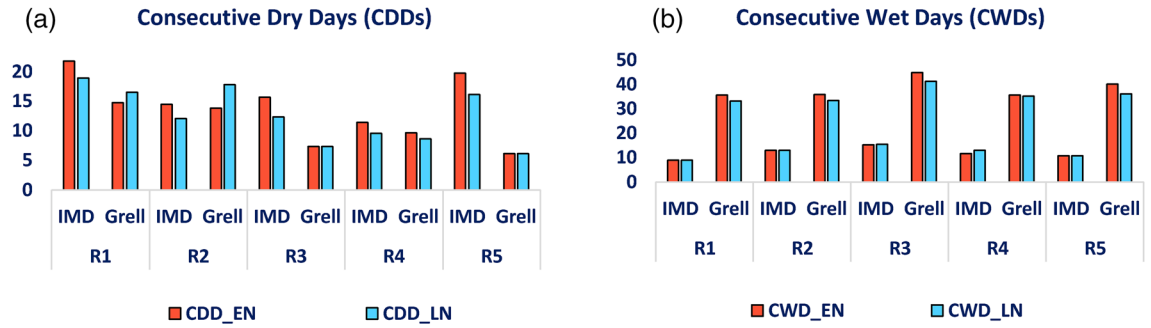

Figure 13. (a and b) The average CDD and CWD of IMD and Grell CPS of RegCM4 during El Nino and La Nina over different subregions of India. CDD, consecutive dry day; CWD, consecutive wet day; IMD, India Meteorological Department; CPS, cumulus parameterization scheme.

Data Availability Statement

The India Meteorological Department (IMD)'s observed daily gridded rainfall data (IMD4) from 1986 to 2010 at a high spatial resolution (0.25° × 0.25°) have been used in this study over Indian domain which are available through the "Data Supply Portal" on payment basis (http://dsp.imdpune.gov.in/). These data are supplied as per IMD's data charging policy by National Data Center IMD, Pune. For initializing and boundary condition, the RegCM4 model, 6 hourly of ECMWF's ERA-Interim reanalysis data (resolution 1.5° × 1.5°) for air temperature, geopotential height, relative humidity, zonal, and meridional wind were collected from the site https://www.ecmwf.int/en/forecasts/datasets/reanalysis-datasets/era-interim and NOAA's Weekly Optimum Interpolation SSTs are downloaded from the site https://www.ncdc.noaa.gov/oisst for 1981–2010.

Acknowledgments
This work is a part of an R&D project, funded by DST, Govt. of India in the form of the Center for Excellence in Climate Change. The corresponding author would like to thank the funding support from the University Grants Commission in the form of Junior Research Fellowship. The authors are grateful to the India Meteorological Department (IMD) for providing necessary facility to collect rainfall data and NCAR for providing Era-Interim reanalysis data set. Authors are thankful to ICTP, Italy, for providing RegCM4 for the dynamical downscaling.

References

Aldrian, E., Gates, L. D., & Widodo, F. H. (2007). Seasonal variability of Indonesian rainfall in ECHAM4 simulations and in the reanalyses: The role of ENSO. *Theoretical and Applied Climatology*, *87*(1–4), 41–59.

Anthes, R. A. (1977). A cumulus parameterization scheme utilizing a one-dimensional cloud model. *Monthly Weather Review*, *105*(3), 270–286.

Arini, E. Y., Hidayat, R., & Faqih, A. (2015). Rainfall simulation using RegCM4 model in Kalimantan during El Nino Southern Oscillation. *Procedia Environmental Sciences*, *24*, 70–86.

Ashfaq, M., Shi, Y., Tung, W. W., Trapp, R. J., Gao, X., Pal, J. S., & Diffenbaugh, N. S. (2009). Suppression of south Asian summer monsoon precipitation in the 21st century. *Geophysical Research Letters*, *36*, L01704. https://doi.org/10.1029/2008GL036500

Ashok, K., Guan, Z., Saji, N. H., & Yamagata, T. (2004). Individual and combined influences of ENSO and the Indian Ocean dipole on the Indian summer monsoon. *Journal of Climate*, *17*(16), 3141–3155.

Ashok, K., Guan, Z., & Yamagata, T. (2001). Impact of the Indian Ocean dipole on the relationship between the Indian monsoon rainfall and ENSO. *Geophysical Research Letters*, *28*(23), 4499–4502.

Bao, Y. (2013). Simulations of summer monsoon climate over East Asia with a Regional Climate Model (RegCM) using Tiedtke convective parameterization scheme (CPS). (*Atmospheric Research*, *134*, 35–44. https://doi.org/10.1016/j.atmosres.2013.06.009

Bhatla, R., Ghosh, S., Mall, R. K., Sinha, P., & Sarkar, A. (2018). Regional climate model performance in simulating intra-seasonal and interannual variability of Indian summer monsoon. *Pure and Applied Geophysics*, *175*(10), 3697–3718.

Bhatla, R., Ghosh, S., Mandal, B., Mall, R. K., & Sharma, K. (2016). Simulation of Indian summer monsoon onset with different parameterization convection schemes of RegCM-4.3. *Atmospheric Research*, *176*, 10–18.

Bhatla, R., Ghosh, S., Verma, S., Mall, R. K., & Gharde, G. R. (2019). Variability of monsoon over homogeneous regions of India using regional climate model and impact on crop production. *Agricultural Research*, *8*(3), 331–346.

Bhatla, R., Mandal, B., Verma, S., Ghosh, S., & Mall, R. K. (2019). Performance of regional climate model in simulating monsoon onset over Indian subcontinent. *Pure and Applied Geophysics*, *176*(1), 409–420.

Bhatla, R., Verma, S., Ghosh, S., & Mall, R. K. (2020). Performance of regional climate model in simulating Indian summer monsoon over Indian homogeneous region. *Theoretical and Applied Climatology*, *139*(3), 1121–1135.

Cai, W., Borlace, S., Lengaigne, M., Van Rensch, P., Collins, M., Vecchi, G., et al. (2014). Increasing frequency of extreme El Niño events due to greenhouse warming. *Nature Climate Change*, *4*(2), 111–116.

Chang, C. P., Harr, P., & Ju, J. (2001). Possible roles of Atlantic circulations on the weakening Indian monsoon rainfall–ENSO relationship. *Journal of Climate*, *14*(11), 2376–2380.

Chang, H. I., Kumar, A., Niyogi, D., Mohanty, U. C., Chen, F., & Dudhia, J. (2009). The role of land surface processes on the mesoscale simulation of the July 26, 2005 heavy rain event over Mumbai, India. *Global and Planetary Change*, *67*(1–2), 87–103.

Da Rocha, R. P., Reboita, M. S., Dutra, L. M. M., Llopart, M. P., & Coppola, E. (2014). Interannual variability associated with ENSO: Present and future climate projections of RegCM4 for South America-CORDEX domain. *Climatic Change*, *125*(1), 95–109.

Dash, S. K., Pattnayak, K. C., Panda, S. K., Vaddi, D., & Mamgain, A. (2015). Impact of domain size on the simulation of Indian summer monsoon in RegCM4 using mixed convection scheme and driven by HadGEM2. *Climate Dynamics*, *44*(3–4), 961–975.

Dash, S. K., Shekhar, M. S., & Singh, G. P. (2006). Simulation of Indian summer monsoon circulation and rainfall using RegCM3. *Theoretical and Applied Climatology*, *86*(1–4), 161–172.
Davis, M. (2001). *Late Victorian holocausts: El Niño famines and the making of the third world*. ISBN 978-1-85984-739-8, Verso Books. https://archive.org/details/latevictorianhol00dav_wbr/page/9/mode/2up
Davis, N., Bowden, J., Semazzi, F., Xie, L., & Önol, B. (2009). Customization of RegCM3 regional climate model for eastern Africa and a tropical Indian Ocean domain. *Journal of Climate*, *22*(13), 3595–3616.
Dickinson, R. E., Henderson-Sellers, A., & Kennedy, P. J. (1993). Biosphere atmosphere transfer scheme (BATS) version 1e as coupled to the NCAR community climate model. NCAR Tech. Note TH-387+ STR p. 72.
Emanuel, K. A. (1991). A scheme for representing cumulus convection in large-scale models. *Journal of the Atmospheric Sciences*, *48*(21), 2313–2329.
Field, C. B., Barros, V., Stocker, T. F., & Dahe, Q. (Eds.), (2012). *Managing the risks of extreme events and disasters to advance climate change adaptation: Special report of the intergovernmental panel on climate change*. Cambridge University Press.
Frich, P., Alexander, L. V., Della-Marta, P. M., Gleason, B., Haylock, M., Tank, A. K., & Peterson, T. (2002). Observed coherent changes in climatic extremes during the second half of the twentieth century. *Climate Research*, *19*(3), 193–212.
Gao, X., Shi, Y., Zhang, D., Wu, J., Giorgi, F., Ji, Z., & Wang, Y. (2012). Uncertainties in monsoon precipitation projections over China: Results from two high-resolution RCM simulations. *Climate Research*, *52*, 213–226.
Gao, X. J., Zhao, Z. C., Ding, Y. H., Huang, R. H., & Filippo, G. (2001). Climate change due to greenhouse effects in China as simulated by a regional climate model. *Advances in Atmospheric Sciences*, *18*, 1224–1230.
Ghosh, S., Bhatla, R., Mall, R. K., Srivastava, P. K., & Sahai, A. K. (2019). Aspect of ECMWF downscaled Regional Climate Modeling in simulating Indian summer monsoon rainfall and dependencies on lateral boundary conditions. *Theoretical and Applied Climatology*, *135*(3–4), 1559–1581.
Giorgi, F. (2006). Regional climate modeling: Status and perspectives. *Journal de Physique IV (Proceedings)*, *139*, 101–118.
Giorgi, F. (2019). Thirty years of regional climate modeling: Where are we and where are we going next?. *Journal of Geophysical Research: Atmospheres*, *124*, 5696–5723. https://doi.org/10.1029/2018JD030094
Giorgi, F., Coppola, E., Solmon, F., Mariotti, L., Sylla, M. B., Bi, X., et al. (2012). RegCM4: Model description and preliminary tests over multiple CORDEX domains. *Climate Research*, *52*, 7–29.
Goswami, B. N. (1998). Physics of ENSO–monsoon connection. *Indian Journal of Marine Sciences*, *27*, 82–89.
Grell, G. A. (1993). Prognostic evaluation of assumptions used by cumulus parameterizations. *Monthly Weather Review*, *121*(3), 764–787.
Guhathakurta, P., & Rajeevan, M. (2006). *Trends in the rainfall pattern over India* (NCC Res. Rep. 2, pp. 1–25). Pune, India: National Climate Centre, India Meteorological Department. http://www.hpccc.gov.in/PDF/Rainfall/NCC%20Research%20Report.pdf
Holtslag, A. A. M., & Boville, B. A. (1993). Local versus nonlocal boundary-layer diffusion in a global climate model. *Journal of Climate*, *6*(1O), 1825–1842.
Holtslag, A. A. M., De Bruijn, E. I. F., & Pan, H. L. (1990). A high resolution air mass transformation model for short-range weather forecasting. *Monthly Weather Review*, *118*(8), 1561–1575.
Huang, W. R., Chan, J. C., & Au-Yeung, A. Y. (2013). Regional climate simulations of summer diurnal rainfall variations over East Asia and Southeast China. *Climate Dynamics*, *40*(7–8), 1625–1642.
Hung, M. P., Lin, J. L., Wang, W., Kim, D., Shinoda, T., & Weaver, S. J. (2013). MJO and convectively coupled equatorial waves simulated by CMIP5 climate models. *Journal of Climate*, *26*(17), 6185–6214.
Jones, P. D., Raper, S. C. B., Bradley, R. S., Diaz, H. F., Kelly, P. M., & Wigley, T. M. L. (1986). Northern Hemisphere surface air temperature variations: 1851–1984. *The Journal of Applied Meteorology and Climatology*, *25*, 161–179.
Kiehl, J. T., Hack, J. J., Boville, B. A., & Briegleb, B. P. (1996). Description of the NCAR community climate model (CCM3). Technical Note (No. PB-97-131528/XAB; NCAR/TN-420-STR). *Technical Note (No. PB-97-131528/XAB; NCAR/TN-420-STR)*, (United States): National Center for Atmospheric Research Boulder CO (United States). https://www.osti.gov/biblio/442361
Kripalani, R. H., & Kulkarni, A. (1997). Rainfall variability over South–east Asia—connections with Indian monsoon and ENSO extremes: new perspectives. *International Journal of Climatology*, *17*(11), 1155–1168.
Kripalani, R. H., & Kulkarni, A. (2001). Monsoon rainfall variations and teleconnections over South and East Asia. *International Journal of Climatology*, *21*(5), 603–616.
Kripalani, R. H., Oh, J. H., & Chaudhari, H. S. (2007). Response of the East Asian summer monsoon to doubled atmospheric CO_2: Coupled climate model simulations and projections under IPCC AR4. *Theoretical and Applied Climatology*, *87*(1–4), 1–28.
Kripalani, R. H., Singh, S. V., Vernekar, A. D., & Thapliyal, V. (1996). Empirical study on Nimbus-7 snow mass and Indian summer monsoon rainfall. *International Journal of Climatology*, *16*(1), 23–34.
Kumar, K. K., Rajagopalan, B., & Cane, M. A. (1999). On the weakening relationship between the Indian monsoon and ENSO. *Science*, *284*(5423), 2156–2159.
Lin, J. L., Kiladis, G. N., Mapes, B. E., Weickmann, K. M., Sperber, K. R., Lin, W., et al. (2006). Tropical intraseasonal variability in 14 IPCC AR4 climate models. Part I: Convective signals. *Journal of Climate*, *19*(12), 2665–2690.
Lin, J. L., Weickman, K. M., Kiladis, G. N., Mapes, B. E., Schubert, S. D., Suarez, M. J., et al. (2008). Subseasonal variability associated with Asian summer monsoon simulated by 14 IPCC AR4 coupled GCMs. *Journal of Climate*, *21*(18), 4541–4567.
Naidu, C. V., Satyanarayana, G. C., Rao, L. M., Durgalakshmi, K., Raju, A. D., Kumar, P. V., & Mounika, G. J. (2015). Anomalous behavior of Indian summer monsoon in the warming environment. *Earth-Science Reviews*, *150*, 243–255.
Nayak, S., Mandal, M., & Maity, S. (2019). Performance evaluation of RegCM4 in simulating temperature and precipitation climatology over India. *Theoretical and Applied Climatology*, *137*(1–2), 1059–1075.
Pai, D. S., Sridhar, L., Rajeevan, M., Sreejith, O. P., Satbhai, N. S., & Mukhopadhyay, B. (2014). Development of a new high spatial resolution (0.25 × 0.25) long period (1901–2010) daily gridded rainfall data set over India and its comparison with existing data sets over the region. *Mausam*, *65*(1), 1–18.
Pal, J. S., Giorgi, F., Bi, X., Elguindi, N., Solmon, F., Gao, X., et al. (2007). Regional climate modeling for the developing world: The ICTP RegCM3 and RegCNET. *Bulletin of the American Meteorological Society*, *88*(9), 1395–1410.
Pal, J. S., Small, E. E., & Eltahir, E. A. (2000). Simulation of regional-scale water and energy budgets: Representation of subgrid cloud and precipitation processes within RegCM. *Journal of Geophysical Research*, *105*(D24), 29579–29594.
Parthasarathy, B., Munot, A. A., & Kothawale, D. R. (1994). All-India monthly and seasonal rainfall series: 1871–1993. *Theoretical and Applied Climatology*, *49*(4), 217–224.
Rajeevan, M., & Bhate, J. (2009). A high resolution daily gridded rainfall dataset (1971–2005) for mesoscale meteorological studies. *Current Science*, 558–562.

Rajeevan, M., Unnikrishnan, C. K., Niranjan Kumar, K., & Sreekala, P. P. (2012). Northeast monsoon over India: variability and prediction. *Meteorological Applications*, *19*(2), 226–236.
Raju, P. V. S., Bhatla, R., Almazroui, M., & Assiri, M. (2015). Performance of convection schemes on the simulation of summer monsoon features over the South Asia CORDEX domain using RegCM-4.3. *International Journal of Climatology*, *35*(15), 4695–4706.
Ratnam, J. V., Behera, S. K., Ratna, S. B., Rautenbach, C. D. W., Lennard, C., Luo, J. J., et al. (2013). Dynamical downscaling of austral summer climate forecasts over southern Africa using a regional coupled model. *Journal of Climate*, *26*(16), 6015–6032.
Ratnam, J. V., Giorgi, F., Kaginalkar, A., & Cozzini, S. (2009). Simulation of the Indian monsoon using the RegCM3–ROMS regional coupled model. *Climate Dynamics*, *33*(1), 119–139.
Reynolds, R. W., Smith, T. M., Liu, C., Chelton, D. B., Casey, K. S., & Schlax, M. G. (2007). Daily high-resolution-blended analyses for sea surface temperature. *Journal of Climate*, *20*(22), 5473–5496.
Roxy, M. K., Ritika, K., Terray, P., Murtugudde, R., Ashok, K., & Goswami, B. N. (2015). Drying of Indian subcontinent by rapid Indian Ocean warming and a weakening land–sea thermal gradient. *Nature Communications*, *6*(1), 1–10.
Sabin, T. P., Krishnan, R., Ghattas, J., Denvil, S., Dufresne, J. L., Hourdin, F., & Pascal, T. (2013). High resolution simulation of the South Asian monsoon using a variable resolution global climate model. *Climate Dynamics*, *41*(1), 173–194.
Sahai, A. K., Pattanaik, D. R., Satyan, V., & Grimm, A. M. (2003). Teleconnections in recent time and prediction of Indian summer monsoon rainfall. *Meteorology and Atmospheric Physics*, *84*(3–4), 217–227.
Saji, N. H., Goswami, B. N., Vinayachandran, P., & Yamagata, T. (1999). A dipole mode in the tropical Indian Ocean. *Nature*, *401*, 360–363.
Sanap, S. D., Priya, P., Sawaisarje, G. K., & Hosalikar, K. S. (2019). Heavy rainfall events over southeast peninsular India during northeast monsoon: Role of El Niño and easterly wave activity. *International Journal of Climatology*, *39*(4), 1954–1968.
Selvaraju, R. (2003). Impact of El Niño–southern oscillation on Indian foodgrain production. *International Journal of Climatology*, *23*(2), 187–206.
Seth, A., Rauscher, S. A., Camargo, S. J., Qian, J. H., & Pal, J. S. (2007). RegCM3 regional climatologies for South America using reanalysis and ECHAM global model driving fields. *Climate Dynamics*, *28*(5), 461–480.
Shukla, J. (1987). Interannual variability of monsoons. *Monsoons*, 399–464.
Sikka, D. R. (1980). Some aspects of the large scale fluctuations of summer monsoon rainfall over India in relation to fluctuations in the planetary and regional scale circulation parameters. *Proceedings of the Indian Academy of Sciences - Earth and Planetary Sciences*, *89*, 179–195.
Simmons, A. (2006). ERA-Interim: New ECMWF reanalysis products from 1989 onwards. *ECMWF Newsletter*, *110*, 25–36.
Sinha, P., Mohanty, U. C., Kar, S. C., Dash, S. K., & Kumari, S. (2013). Sensitivity of the GCM driven summer monsoon simulations to cumulus parameterization schemes in nested RegCM3. *Theoretical and Applied Climatology*, *112*(1–2), 285–306.
Sylla, M. B., Giorgi, F., Coppola, E., & Mariotti, L. (2013). Uncertainties in daily rainfall over Africa: Assessment of gridded observation products and evaluation of a regional climate model simulation. *International Journal of Climatology*, *33*(7), 1805–1817.
Tiedtke, M. (1989). A comprehensive mass flux scheme for cumulus parameterization in large-scale models. *Monthly Weather Review*, *117*(8), 1779–1800.
Turner, A. G., & Annamalai, H. (2012). Climate change and the South Asian summer monsoon. *Nature Climate Change*, *2*(8), 587–595.
Varikoden, H., Revadekar, J. V., Choudhary, Y., & Preethi, B. (2015). Droughts of Indian summer monsoon associated with El Niño and Non-El Niño years. *International Journal of Climatology*, *35*(8), 1916–1925.
Walker, G. T. (1925). Correlation in seasonal variations of weather—A further study of world weather. *Monthly Weather Review*, *53*(6), 252–254.
Webster, P. J., & Yang, S. (1992). Monsoon and ENSO: Selectively interactive systems. *Quarterly Journal of the Royal Meteorological Society*, *118*(507), 877–926.
World Meteorological Association. (2013). *The Global Climate 2001–2010: A decade of climate extremes, summary report* (WMO-No. 1103). Geneva, Switzerland.
Yang, J., Liu, Q., Xie, S. P., Liu, Z., & Wu, L. (2007). Impact of the Indian Ocean SST basin mode on the Asian summer monsoon. *Geophysical Research Letters*, *34*, L02708. https://doi.org/10.1029/2006GL028571
Zeng, X., Zhao, M., & Dickinson, R. E. (1998). Intercomparison of bulk aerodynamic algorithms for the computation of sea surface fluxes using TOGA COARE and TAO data. *Journal of Climate*, *11*(10), 2628–2644.
Zhang, X., Alexander, L., Hegerl, G. C., Jones, P., Tank, A. K., Peterson, T. C., et al. (2011). Indices for monitoring changes in extremes based on daily temperature and precipitation data. *Wiley Interdisciplinary Reviews Climate Change*, *2*(6), 851–870. https://doi.org/10.1002/wcc.147
Zou, L., Qian, Y., Zhou, T., & Yang, B. (2014). Parameter tuning and calibration of RegCM3 with MIT–Emanuel cumulus parameterization scheme over CORDEX East Asia domain. *Journal of Climate*, *27*(20), 7687–7701.